Summer Monsoon Rainfall Variability in Central China over the Past 4700 Years and Its Possible Link to Solar Activity

Jingwei ZHANG[1,2,3], Kan ZHAO[2*], Xinggong KONG[2], Yongjin WANG[2], Xianfang WANG[4], Shushuang LIU[2], Zhenjun WANG[2], Hai CHENG[5], and R. Lawrence EDWARDS[2,6]

1 *School of Geography and Environment, Jiangxi Normal University, Nanchang* 330022, *China*
2 *School of Geography Science, Nanjing Normal University, Nanjing* 210023, *China*
3 *Key Laboratory of Poyang LakeWetland and Watershed Research of Ministry of Education, Jiangxi Normal University, Nanchang* 330022, *China*
4 *Lanling NO.4 Middle School, Linyi* 277700, *China*
5 *Institute of Global Environmental Change, Xi'an Jiaotong University, Xi'an* 710049, *China*
6 *Department of Geology and Geophysics, University of Minnesota, Minneapolis MN*55455, *USA*

(Received September 25, 2020; in final form April 2, 2021)

ABSTRACT

Based on 467 pairs of $\delta^{18}O$ and $\delta^{13}C$ records and 8 ^{230}Th dates from a stalagmite (BF4) from Xiniu Cave, central China, we present a reconstruction of ~9-yr resolution monsoon rainfall record for the past 4700 years. Our $\delta^{18}O$ record shows good coherence with East Asian summer monsoon (EASM) rainfall proxies from adjacent regions during the overlapping intervals, suggesting that $\delta^{18}O$ signal in BF4 can be interpreted as a monsoon rainfall proxy. The $\delta^{13}C$ variations are related to changes in local processes at the cave site, and regional rainfall and temperature changes. Based on the $\delta^{18}O$ record, a series of dry periods can be identified at 4500–4200, 3500–3200, 2800–2500, 1900–1600, 1400–1200, 700–500, and 400–200 yr BP, while a series of wet periods can be identified at 4200–3600, 2400–2200, 3200–2800, 1100–900, 600–400, and 200–100 yr BP. Power spectrum analysis on our $\delta^{18}O$ record reveals significant cycles at ~470 and ~80 yr, coinciding with the typical solar periodic variations. This result suggests that changes in solar activity play a dominant role in driving centennial–decadal monsoon rainfall variation in central China. Due to minor changes in solar irradiance (less than 1.5 W m^{-2}) over the past 4700 years, our record was further compared to the El Niño–Southern Oscillation (ENSO) and Pacific Decadal Oscillation (PDO) proxies, confirming that solar forcing on monsoon rainfall changes might be amplified by the ENSO and PDO variations. From 600 to 150 yr BP (the Little Ice Age, LIA), a positive shift of ~2‰ can be revealed in both the $\delta^{18}O$ and $\delta^{13}C$ records, indicating a cold/dry climatic pattern. By comparing our $\delta^{18}O$ and $\delta^{13}C$ records with historical documents, we suggest that the climatic deteriorations between 450 and 250 yr BP may have caused serious social unrest at the end of the Ming Dynasty.

Key words: stalagmite record, Xiniu Cave, solar activity, El Niño–Southern Oscillation (ENSO), Pacific Decadal Oscillation (PDO), amplify mechanism, Little Ice Age (LIA)

Citation: Zhang, J. W., K. Zhao, X. G. Kong, et al., 2021: Summer monsoon rainfall variability in central China over the past 4700 years and its possible link to solar activity. *J. Meteor. Res.*, **35**(4), 594–606, doi: 10.1007/s13351-021-0168-1.

1. Introduction

The East Asian summer monsoon (EASM) system is an important component of the Asian monsoon system (Wang and Ho, 2002). A major feature of the EASM is the prevailing southerlies induced by the pressure gradient between the Asian continent and the subtropical oceans. In summer, the EASM carries a large body of water vapor into the inland of China, contributing as much as 60%–70% of the annual rainfall amount in southern and northern China, respectively (Ding et al., 2005, 2018). Changes in the EASM, particularly those

Supported by the National Natural Science Foundation of China (42071105, 41571102, 41931178, 41672164, and 41172314), U.S. Nature Science Foundation (1702816), Project Funded by the Priority Academic Program Development of Jiangsu Higher Education Institutions (164320H116), and 111 Program of China (D19002).

*Corresponding author: 09371@njnu.edu.cn

associated with the occurrence of floods and droughts, therefore have a huge impact on social–economic development and the well-being of the inhabitants in China. To achieve a sustainable level of development in the future, it is essential to improve our knowledge of the nature of the EASM variations and the underlying dynamical mechanisms.

On centennial to multidecadal timescales, solar changes were considered to be a key driver of the Holocene EASM changes (Wang et al., 2005; Zhang et al., 2008). However, more evidence is emerging that the solar forcing of the EASM variations may not be through the direct heating. It is more likely that solar variations lead to changes in atmospheric or oceanic circulation that amplifies solar initial input (Neff et al., 2001; Emile-Geay et al., 2007). However, the modern meteorological records are too short (extending to the 1950s) to capture the natural long-term variability of climatic phenomena. Consequently, the mediator between sun and the EASM remains less certain. This uncertainty not only impedes our understanding of the EASM behavior in the past, but also limits our ability to predict its variations in the future, especially considering the background of ongoing global warming. To address this issue, more investigations based on long and continuous climatic records from EASM-sensitive regions are expected.

Mt. Shennongjia is located in the northwest of Hubei Province, central China, which is a typical region controlled by the EASM system. This area and adjacent regions serve as the source of water for the middle route of the South-to-North Water Diversion Project (SNWDP) in China (Chen et al., 2007). Therefore, even a small fluctuation in monsoon rainfall resulting from the EASM variability could have a huge impact on the sustainable development of China. At Mt. Shennongjia, the underlying dynamics of the centennial-scale climatic changes during the Holocene have been intensely studied and debated. The traditional interpretation asserts that solar forcing through "high–low latitudes teleconnection" was the dominant cause of this variability (Ma et al., 2008; Dong et al., 2010; Li et al., 2016; Zhang et al., 2019). However, other researchers have instead suggested that low-latitude hydrological processes probably played a more important role (Cui et al., 2012; Zhao K. et al., 2016; Zhang et al., 2018). To improve our understanding of climatic changes during the Holocene and the underlying dynamics, it is necessary to produce additional records to help resolve this controversy.

Stalagmite is an ideal natural archive for geological and historical climatic reconstruction, with the advantages of accurate dating, continuous growth, and high resolution (Cheng et al., 2016). In recent studies, the stable isotope records ($\delta^{18}O$ and $\delta^{13}C$) show a good consistency with the observed monsoon rainfall record in the EASM domain (Tan et al., 2011, 2018a, b), strongly suggesting that the $\delta^{18}O$ record can also be used for monsoon rainfall reconstruction. With this background, we present a new well-dated, approximately 9-yr resolution $\delta^{18}O$ and $\delta^{13}C$ records from a stalagmite that grew in the late Holocene in Xiniu Cave, central China, to reconstruct the monsoon climate changes over the past 4700 years. The two aims of this study are: 1) producing a new record of the EASM rainfall from central China, and 2) investigating the underlying dynamics of centennial–decadal-scale EASM rainfall variations.

2. Regional setting, sample description, and main analysis methods

Xiniu Cave (31°40′45″N, 110°25′13″E, 2012 m above sea level) is on the western face of Mt. Shennongjia, central China (Fig.1). The meteorological records from Fangxian station, which is located approximately 40 km northwest of Xiniu Cave, show that the monthly mean temperature varies from 2.2°C (December–February) to 21.8°C (June–August), with the highest temperature in July (22.8°C) and lowest in January (0.9°C). Rainfall in this region is strongly seasonally dependent due to its location within the mid-subtropical zone, which is strongly influenced by the EASM. During boreal summer (June–September), the inflow of warm/humid air from the tropical ocean reaches the southern slope of Mt. Shennongjia, delivering on average approximately 57% of total annual rainfall (~1000 mm).

Xiniu Cave is a rare alpine cave in monsoonal China, which formed in the limestone bedrock of the simian formation, with a measured length of approximately 200 m. The area above the cave is occupied by forest and the surrounding area consists mainly of temperate deciduous broadleaved plants. We obtained a 240-mm long stalagmite (designated as BF4) in the south of No. 2 entrance of Xiniu Cave. After cutting the stalagmite lengthwise and polishing it, the central growth axis was revealed, showing that the deposition center is relatively stable from bottom to top (Fig. 2a).

For $^{230}Th/U$ dating, eight subsamples, 100–150 mg each, were drilled for dating analysis. The procedures conducted for chemical separation and purification of uranium and thorium are similar to those described in Shao et al. (2019). Measurements were performed on a Finnigan Element inductively coupled plasma mass spectrometer (ICP-MS), equipped with a double-focusing

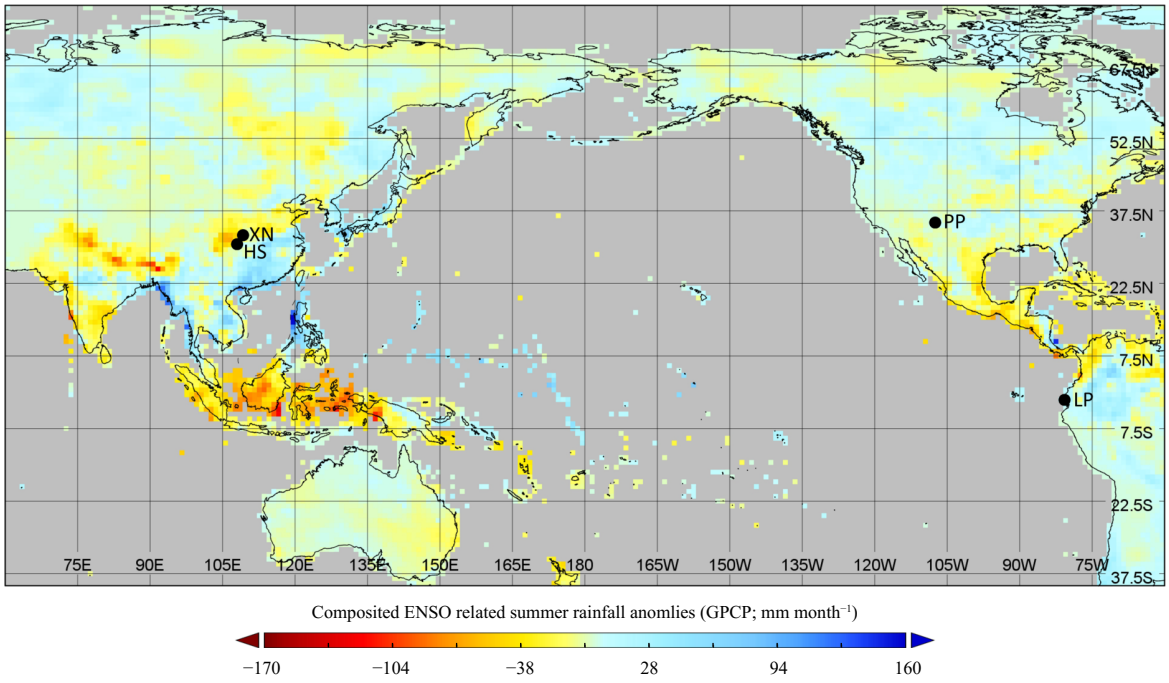

Fig. 1. The composite summer (June–July–August) rainfall anomalies during the El Niño years of 1979–2010 AD (data source from https://www.esrl.noaa.gov/psd/cgi-bin/data/getpage.pl). The main study sites mentioned in this paper are illustrated, which are XN (Xiniu Cave; this study), HS (Heshang Cave; Hu et al., 2008), PP (Pink Panther Cave; Asmerom et al., 2007), and LP (Laguna Pallcacocha Lake; Moy et al., 2002).

sector magnet and energy filter in reversed Nier-Johnson geometry and a MasCom multiplier. This work was operated at the Department of Geology and Geophysics, University of Minnesota, USA. For stable isotopic measurements, 467 subsamples were drilled with a 0.3-mm diameter carbide dental burr at 0.5- and 1.0-mm intervals. The analysis was conducted on a Finnigan-MAT 253 mass spectrometer equipped with an automatic Kiel Carbonate Device at the School of Geography Science, Nanjing Normal University, China. The standards were ran for every 9 subsamples and the duplicates were measured every 15 subsamples to check for reproducibility. The results were reported in parts per mil (‰) relative to the Vienna Pee Dee Belemnite (VPDB) and standardization was accomplished by using NBS-19 ($\delta^{18}O_{VPDB}$ = −2.2‰ and $\delta^{13}C_{VPDB}$ = −1.95‰; Ishimura et al., 2008), with a precision better than 0.06‰ for oxygen and 0.05‰ for carbon at the 2σ level.

3. Results

3.1 *Chronology*

As shown in Table 1, the dating results show high ^{238}U concentrations (from 1782 to 3004 ppb) and low ^{232}Th concentrations (from 74 to 1945 ppt). The age versus depth plot shows that all ^{230}Th ages are in a straitgraphic order within small errors ranging between approximately 7 and 30 yr.

Table 1. U–Th data and ^{230}Th dates for BF4 from Xiniu Cave

Sample number	^{238}U (ppb)	^{230}Th (ppt)	$^{230}Th/^{232}Th$ (activity)	$^{234}U^{a}$ (measured)	$^{230}Th/^{238}U$ (activity)	^{230}Th age (uncorrected; yr BP)	^{230}Th age (corrected; yr BP)
BF4-11	2157.29	140.95	815.89	644.41	0.0032	215 ± 8	**213 ± 8**
BF4-26	3003.89	86.46	3820.50	648.97	0.0067	442 ± 7	**441 ± 7**
BF4-61	2431.85	73.95	6750.57	666.23	0.0124	817 ± 13	**817 ± 13**
BF4-131	2523.59	454.94	2701.75	690.26	0.0295	1920 ± 19	**1917 ± 19**
BF4-144	2419.24	1944.53	914.20	773.96	0.0445	2770 ± 25	**2756 ± 25**
BF4-155	1781.52	1731.95	889.04	648.36	0.0523	3517 ± 28	**3500 ± 30**
BF4-186	2378.69	248.62	9376.87	676.67	0.0594	3927 ± 34	**3925 ± 25**
BF4-216-A	2563.32	799.93	3407.56	637.15	0.0644	4372 ± 26	**4366 ± 26**

The bold values are the ^{230}Th ages used in our age model. Errors are 2σ analytical errors. Decay constant values are $\lambda_{230} = 9.1705 \times 10^{-6}\ yr^{-1}$, $\lambda_{234} = 2.82206 \times 10^{-6}\ yr^{-1}$, and $\lambda_{238} = 1.55125 \times 10^{-10}\ yr^{-1}$. Corrected ^{230}Th ages are calculated by using an estimated initial $^{230}Th/^{232}Th$ atomic ratio of $(4.4 \pm 2.2) \times 10^{-6}$. BP stands for "before present" where the "present" is defined as the year 1950 AD.

The Monte–Carlo simulations and constructing proxy records from age (COPRA) were used to establish the chronology framework (Breitenbach et al., 2012). For processes, the COPRA computed 2000 ensemble realizations for both the $\delta^{18}O$ and $\delta^{13}C$ records, from which the median, such as the central age for a defined sample depth, was calculated. The uncertainty in the age model was defined by the 95 % confidence level, derived by using the ±2σ deviation from the median. The results show that stalagmite BF31 was continuously deposited between 4703 and 50 yr BP (Fig. 2b).

3.2 *Stable isotope records*

Profiles of $\delta^{18}O$ and $\delta^{13}C$, with a mean resolution of ~9 yr, are shown in Fig. 2. The $\delta^{18}O$ value ranges from −10.76‰ to −8.06‰, with a mean value of −9.45‰ (Fig. 2c). The long-term trend of the $\delta^{18}O$ record broadly follows a decrease of Northern Hemisphere summer insolation (NHSI; Bergerand and Loutre, 1991; Fig. 2d). Furthermore, this trend is also interrupted by a series of abnormal swings at centennial scale, with amplitudes of ~1‰ to ~2‰. The $\delta^{13}C$ value ranges from −11.57‰ to −6.0‰, with a mean value of −10.6‰ (Fig. 2e). The observed long-term trend of the $\delta^{18}O$ is absent from the $\delta^{13}C$ record. The most prominent feature of the $\delta^{13}C$ record is an abrupt positive shift between 600 and 100 yr BP. The correlation coefficient for the relationship between the $\delta^{13}C$ and $\delta^{18}O$ records is ~0.23 ($n = 467$, $p < 0.01$; Mudelsee, 2003). When removing the long trend (Taylor, 2000), this value increases to ~0.33.

4. Discussion

4.1 *Climatic interpretations of the stable isotope records*

Before interpreting the stalagmite's $\delta^{18}O$ as a climatic proxy, it needs to be confirmed that the calcite was deposited under isotopic equilibrium fractionation (Hendy, 1971). Following the ideas of Hendy (1971), 30 subsamples from 6 growth layers were analyzed. In detail, neither a statistically significant covariance between $\delta^{18}O$ and $\delta^{13}C$, nor any progressive increases in $\delta^{18}O$ along an individual growth layer were found (Fig. S1A). Moreover, we calculated the correlations between $\delta^{18}O$ and $\delta^{13}C$ along the different growth layers, and the R^2 values are all statistically insignificant (Fig. S2B). These results suggest that kinetic fractionation was insignificant and the $\delta^{18}O$ signal is a primarily of climatic origin (Hendy, 1971). In addition to the Hendy tests, replication among two or more $\delta^{18}O$ profiles from the same or nearby cave is another rigorous test for isotopic equilibrium (Dorale and Liu, 2009). This study, the published

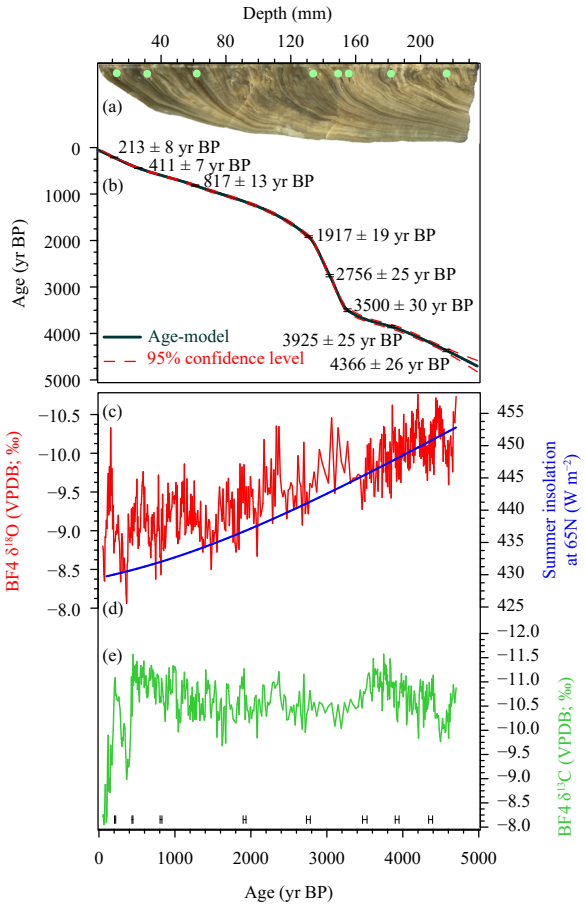

Fig. 2. The photo of stalagmite BF4 and the chronological and isotopic results. (a) Polished sections of stalagmite BF4 collected from Xiniu Cave, (b) the age model for stalagmite BF4 by using COPRA framework (Breitenbach et al., 2012), (c) the records of $\delta^{18}O$ (red curve), and (e) $\delta^{13}C$ (green curve) for stalagmite BF4. Note that the long trend of the $\delta^{18}O$ record broadly tracks (d) the NHSI variations (blue curve; Berger and Loutre, 1991), but a similar pattern is absent in the $\delta^{13}C$ record.

stalagmite $\delta^{18}O$ records from the Xiniu Cave (SN; Li et al., 2010) and Heshang Cave (HS-4; Hu et al., 2008), is introduced for replication test (Dorale and Liu, 2009) and sliding correlation analysis (Zhao L. et al., 2016). In detail, the correlation between BF4 and SN $\delta^{18}O$ profiles is 0.54 ($p < 0.01$; Fig. 3a), and this correlation tends to be stable (the percentage of stability is 42%). A similar strong correlation is also found between BF4 and HS-4 $\delta^{18}O$ profiles ($r = 0.55$, $p < 0.01$; Fig. 3b), with a relatively stable correlation (the percentage of stability is 42%). These results suggest that all stalagmite $\delta^{18}O$ records primary climate signals, although the three stalagmites were deposited under the different flow pathways through the overlying bedrock, groundwater mixing and residence time, CO_2 partial pressure, and degassing history (Dorale and Liu, 2009). In conclusion, both the

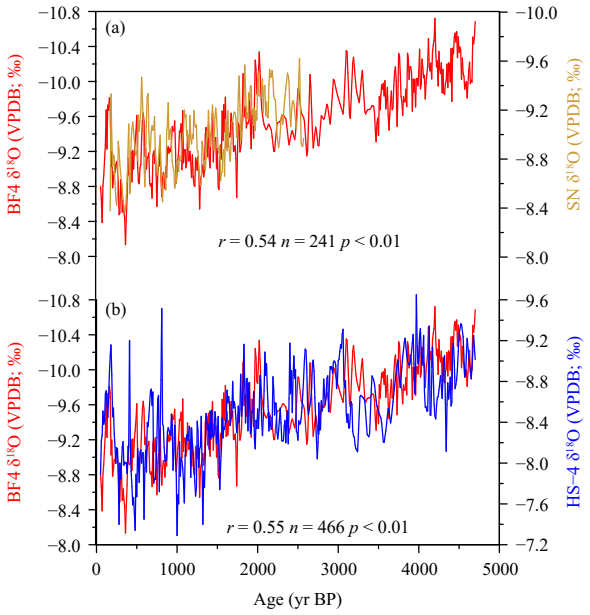

Fig. 3. The replication test. The BF4 $\delta^{18}O$ record (red curve; this study) is chosen to compare with (a) stalagmite SN $\delta^{18}O$ record from Xiniu Cave (brown curve; Li et al., 2010) and (b) stalagmite stalagmite HS-4 $\delta^{18}O$ record from Heshang Cave (blue curve; Hu et al., 2008).

Hendy test and replication test indicate that stalagmite BF4 was deposited under conditions close to isotopic equilibrium fractionation, and its $\delta^{18}O$ variations primarily reflect climatic changes.

On orbital and millennial timescales, Chinese stalagmite $\delta^{18}O$ signals do represent changes in the overall Asian monsoon intensity and/or changes in spatially-integrated rainfall between the cave site and moisture source (Cheng et al., 2016). However, the climatic interpretation at short timescales remains controversial, including the effect of the cave's environment (Cosford et al., 2009), the different source regions of the rainfall (Maher and Thompson, 2012; Tan, 2014), and the amount of regional rainfall (Hu et al., 2008; Zhang et al., 2008; Cai et al., 2010; Tan et al., 2018a, b). Here, two lines of evidence contribute to our understanding of the BF4 $\delta^{18}O$ record as an EASM rainfall proxy. First, the $\delta^{18}O$ record in BF4 bears a remarkable resemblance to the $\delta^{18}O$ record from stalagmite HS-4 from Heshang Cave ($r = 0.55$, $p < 0.01$), indicating that the climatic interpretation of the BF4 $\delta^{18}O$ record is similar to the HS-4 $\delta^{18}O$ record. Li et al. (2018) produced a reliable regional rainfall record ($\delta^{44/42}Ca$) based on a stalagmite from Heshang Cave, which correlates well with both the meteorological data of summer rainfall ($r = -0.34$) and the $\delta^{18}O$ record ($r = 0.36$). Due to a strong correlation between the $\delta^{18}O$ records in BF4 and HS-4 ($r = 0.55$, $p < 0.01$), changes in our $\delta^{18}O$ record may also reflect regional rainfall variations. Second, the BF4 $\delta^{18}O$ record shows an overall similarity with the paleo-hydrological reconstruction from Dajiuhu Lake, Mt. Shennongjia. For example, an increase of the $\delta^{18}O$ values since 4 ka BP is synchronous with high $\delta^{13}C$ values and low total organic carbon (TOC) values resulted from a reduced regional monsoon rainfall (Ma et al., 2008; Zhang et al., 2018). Taking all these discussions together, the good correlations between our $\delta^{18}O$ record and the published monsoon rainfall proxies at the cave site and surroundings, probably indicate that the BF4 $\delta^{18}O$ record can be used as a regional monsoon rainfall proxy, with negative values linked to increased summer monsoon rainfall (or wet condition), and vice versa.

Changes in stalagmite $\delta^{13}C$ values are mainly influenced by local processes, such as C3/C4 vegetation composition (Dorale et al., 1998; McDermott, 2004), vegetative density (Baker et al., 1997; Baldini et al., 2005), soil biomass (Spötl et al., 2005), inorganic processes (Hendy, 1971; Baker et al., 1997; McDermott, 2004), and cave environments (Spötl et al., 2005; Fairchild et al., 2006; Mattey et al., 2008), in a complex manner. Previous studies have demonstrated that these factors are directly or indirectly related to climatic conditions on various timescales (Cosford et al., 2009).

The overlying flora of the Xiniu Cave is composed mainly of C3 plants since the last deglaciation (Ma et al., 2008). The influence of vegetation on $\delta^{13}C$ primarily reflects changes in vegetative density and soil biomass. Under cold and dry conditions, where vegetation is sparse, there is less soil biomass and a lower proportion of light carbon in the dissolution zone, resulting in higher $\delta^{13}C$ values (Baker et al., 1997; Baldini et al., 2005; Zhang J. W. et al., 2019). Local inorganic processes that respond to changes in rainfall and temperature also had a profound impact on our $\delta^{13}C$ records. Under cold and dry conditions, reduced drip rates resulted in higher speleothem $\delta^{13}C$ values owing to more time for CO_2 degassing on the speleothem surface and increased evaporation, enhancing the prior calcite precipitation (PCP) in the unsaturated zone of the karst aquifer (McDermott, 2004; Fairchild et al., 2006). Cave ventilation is another important factor that affects the $\delta^{13}C$ variations (Spötl et al., 2005; Mattey et al., 2008). Stalagmite BF4 was collected approximately 100 m away from the cave's entrance, where the cave air temperature remains stable throughout the year. In winter, enhanced air exchange may have occurred between the cold and dense air outside and the cave atmosphere. This may result in lower pCO_2 of the cave air, increased degassing, and enriched the precipitat-

ing calcite in ^{13}C, and may ultimately produce a higher $\delta^{13}C$ value (Mattey et al., 2008).

Therefore, higher $\delta^{13}C$ values in BF4 generally reflect the diminished vegetative cover and biological production, lower drip rates, and enhanced cave air ventilation at the cave site, associated with decreased rainfall and temperature at local scale, and vice versa. Analyses of the modern climate in central China suggest that changes in rainfall and temperature are mainly controlled by the EASM variability. When the EASM strengthens, the sufficiently warm and wet flow may contribute to robust vegetative growth and biological production, increased drip rates, and weakened cave air ventilation (Cosford et al., 2009; Zhang et al., 2020). The opposite situation could arise when the EASM is weakened and the winter monsoon is strengthened. Therefore, we propose that changes in our $\delta^{13}C$ records primarily reflect regional rainfall and temperature variations, which are closely related to the EASM variability.

4.2 *Monsoon rainfall variations in central China over the past 4700 years*

Our $\delta^{18}O$ record shows that monsoon rainfall in central China has generally decreased over the past 4700 years. To better reveal the timing of centennial monsoon rainfall variations, we removed the long-term trend of our $\delta^{18}O$ record ($\delta^{18}O_d$) and define the new parameter of $\delta^{18}O_d$ value $\geqslant \delta^{18}O_{d\text{-}mean} + 0.5\sigma$‰ (where $\delta^{18}O_{d\text{-}mean}$ is 0.05‰ and σ is the standard deviation, σ = 0.287) as a reduced rainfall signal (Fig. 4a). From this, a series of drought intervals can be identified at 4500–4200, 3500–3200, 2800–2500, 1900–1600, 1400–1200, 700–500, and 400–200 yr BP. By contrast, a series of wet intervals can be identified at 4200–3600, 2400–2200, 3200–2800, 1100–900, 600–400, and 200–100 yr BP. Another remarkable feature is that the occurrence of severe droughts has become more frequent over the last 2500 years.

In frequency, the $\delta^{18}O$ record in BF4 yields significant periodicities of ~467, ~78, ~36, ~3, and ~2 yr (at a 95% confidence level), respectively (Fig. 4b). shorter cycles, including ~36, ~3, and ~2 yr, will not be considered because the mean resolution of our $\delta^{18}O$ record is 9 yr/subsample. The ~470-yr cycle was previously reported from Dongge and Heshang Cave records (Wang et al., 2005; Zhu et al., 2017), and is one of the significant components of solar periodic variation (Stuiver and Becker, 1993). The ~80-yr cycle matches well with the Gleissberg solar activity cycle of ~80 yr, and is also seen in the stalagmite records from monsoonal China (Cosford et al., 2008; Zhang et al., 2013). Hence, our observations support the idea that changes in solar activity played a key role in modulating the monsoon rainfall variability on centennial and decadal timescales.

Solar radiation is the primary source of energy that drives atmospheric–oceanic flow, and it is often invoked

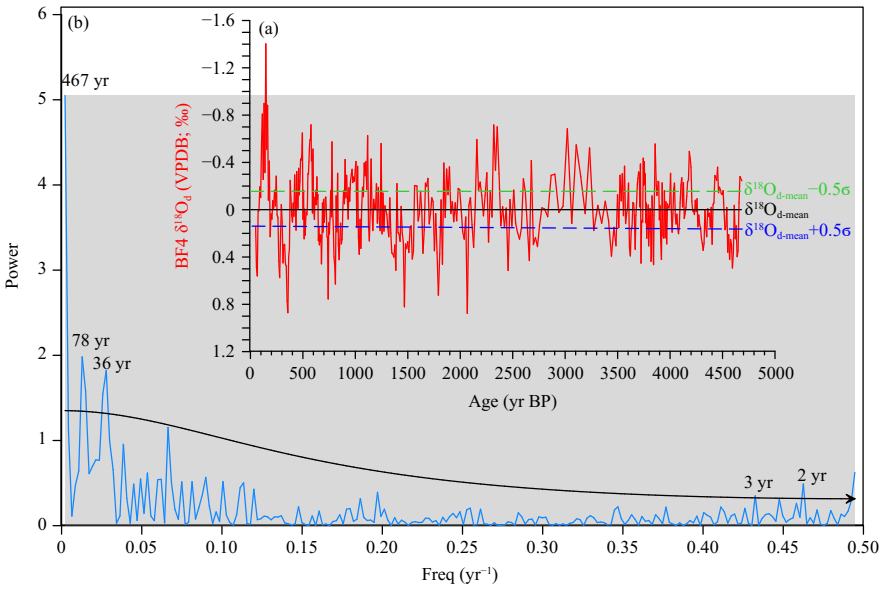

Fig. 4. (a) The $\delta^{18}O_d$ record of stalagmite BF4 (red curve); the green (blue) dotted line represents the $\delta^{18}O_{d\text{-}mean} - 0.5\sigma$ ($\delta^{18}O_{d\text{-}mean} + 0.5\sigma$) of the BF4 time series; the $\delta^{18}O_d$ value $\geqslant \delta^{18}O_{d\text{-}mean} - 0.5$ ($\delta^{18}O_{d\text{-}mean} + 0.5$)‰ is interpreted as an increased (a decreased) monsoon rainfall signal. (b) Power spectral analysis of the BF4 $\delta^{18}O$ record. Spectral peaks are labeled with their cycles (yr) that are above the 95% confidence level (black curve). The spectra were calculated with software past.

to explain natural climate change (Gray et al., 2010; Xiao and Huo, 2016). In China, some recent studies have demonstrated that the solar 11-yr cycle exhibits strong impacts on summer rainfall variation, while the El Niño–Southern Oscillation (ENSO)-related sea surface temperature (SST) anomalies also have an important impact (Wang and Zhao, 2012; Zhou and Chen, 2012; Li et al., 2019). To test this idea further, the BF4 $\delta^{18}O$ record is compared to the total solar irradiance (TSI) record, a typical solar activity proxy (Steinhilber et al., 2009; Fig. 5a). The result indicates that low TSI values are well correlated with monsoon failures (droughts) as revealed by the positive shifts in the BF4 $\delta^{18}O$ record (Fig. 5d). In addition, the BF4 $\delta^{18}O$ and TSI records show a strong correlation, $r = -0.42$ ($n = 466$, $p < 0.01$) for the entire record, supporting the idea that changes in the EASM rainfall are closely related to changes in the solar activity. However, one puzzling fact is that the TSI changes did not yield amplitudes greater than 1.5 W m^{-2} over the past 4700 years. Such a shift only accounts for ~0.1% of the sun's total energy output as proposed by Foukal et al. (2006), and seems too small to directly induce the climate changes. Therefore, other controlling factors might amplify the solar ultimately trigger the climate changes in EASM domain.

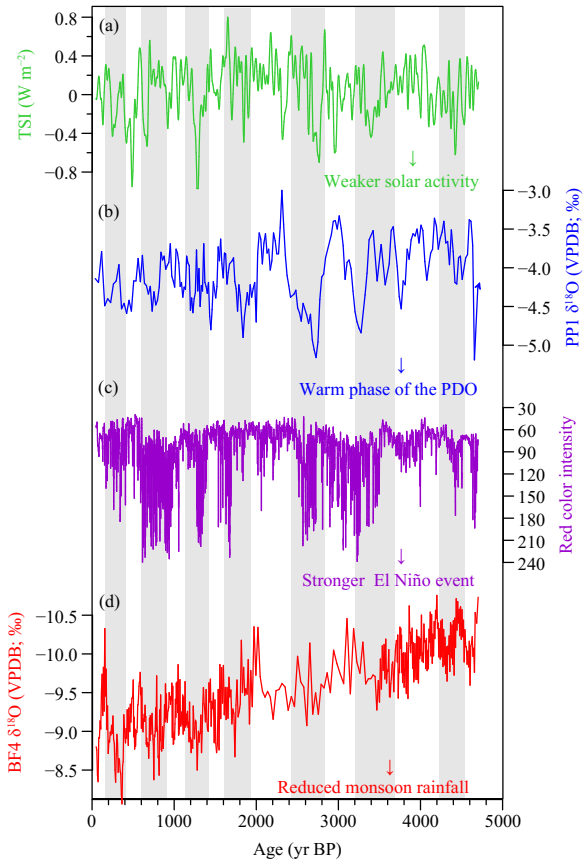

Fig. 5. Comparison of (d) the BF4 $\delta^{18}O$ record (red curve; this study) with (a) TSI record (green curve; Steinhilber et al., 2009), (b) stalagmite PP1 $\delta^{18}O$ record from North America, a proxy for the PDO (blue curve; Asmerom et al., 2007), and (c) the RCI record from EEP, a proxy for ENSO activity (purple curve; Moy et al., 2002).

By defining the rain belt meridional shift index (RMSI), Zhao et al. (2017) investigated the relationship between sunspot number (SNN) and summer rainfall in China. Cross-wavelet analysis shows that changes in RMSI are primarily dominated by the ENSO's 5-yr cycle and the SNN's 11-yr cycle, indicating that the ENSO amplifies small solar signals through a so-called "bottom-up" mechanism (Meehl et al., 2001; van Loon and Meehl, 2012). This mechanism works as: increased solar over cloud-free regions of the subtropics translates into greater evaporation, and moisture convergence and rainfall in the Intertropical Convergence Zone (ITCZ) and South Pacific Convergence Zone (SPCZ), and stronger trades, and cooler SST in the eastern equatorial Pacific (EEP; Meehl et al., 2009). To be one of the most important coupled oceanic–atmospheric modes in the tropical Pacific Ocean region, ENSO powers China's summer rainfall variability on annual timescale by influencing the intensity and mean position of the western Pacific subtropical high (WPSH; Rasmusson and Carpenter, 1983; Ropelewski and Halpert, 1996; Shi and Wang, 2019). To be a long-lived ENSO signal, the Pacific Decadal Oscillation (PDO) is a leading mode of decadal scale variability in SST in the extratropical North Pacific (Mantua et al., 1997). Based on the analysis of the observations and model results, strong correlations were found between the ENSO/PDO and EASM rainfall in China (Yu, 2013; Yu et al., 2015). For examples, Chen (2002) and Chen et al. (2013) found that the ENSO-related monsoon change is strongly modulated by the PDO. There also tends to be a much stronger EASM after a weak East Asian winter monsoon (EAWM) during warm phase of the PDO.

To confirm this idea, we compared the BF4 $\delta^{18}O$ record with the stalagmite (PP1) $\delta^{18}O$ record from North America (as a proxy for the PDO; Asmerom et al., 2007), and the red color intensity (RCI) record from the EEP (as a proxy for the ENSO activity; Moy et al., 2002). As shown in Fig. 5, the identified reduced monsoon rainfall intervals over the past 4700 years (Fig. 5d) were coincident with more negative shifts in the PP1 $\delta^{18}O$ record from North America (indicating a warm phase of the PDO; Fig. 5b) and higher RCI values from the EEP (indicating El Niño conditions; Fig. 5c). These observations suggest that the reduced EASM rainfall is probably related to warm phase of the PDO, as well as to the stronger El Niño events, similar to the modern observations. Hence,

our record provides a new case that changes in ENSO/PDO can amplify solar's initial output, that is, even a minor change in solar activity would probably have a huge effect on climate changes in East Asia.

4.3 *Drought during the Little Ice Age (LIA) and its influence on China's social evolution*

The temporal range of the LIA considered in this study is defined as the period between 500 and 150 yr BP (IPCC, 2007; Fig. 6a). As mentioned above, during the LIA, the $\delta^{18}O$ values range from −10.4‰ to −8.0‰, with a shift of 2.4‰. The $\delta^{18}O$ values reached a maximum between 400 and 280 yr BP, which may indicate an interval of severe drought conditions (Fig. 6h). In addition, the $\delta^{13}C$ values sharply increased from −11.0‰ to −8.5‰ (Fig. 6g), possibly suggesting decreased vegetative cover and biological production, lower drip rates, and enhanced cave ventilation, which in turn reflects a dry/cold climate. The consistency between the two isotopic records in BF4 suggests that the LIA in central China displays an overall dry/cold pattern.

Dry/cold conditions during the LIA are also revealed in a large body of climatic proxies at Mt. Shennongjia. For example, the $\delta^{18}O$ record from Yongxing Cave began to increase from 450 yr BP and reached its maximum at approximately 200 yr BP, indicating a peak drought within this interval (Zhang W. H. et al., 2019). A high resolution stalagmite record from Heilong Cave suggested that, the $\delta^{18}O$ and $\delta^{13}C$ values were relatively higher, and the growth rate was lower between 600 and 150 yr BP, indicating drier conditions than normal (Cui et al., 2012). The lowest diatom turnover and carbon sequestration in Yichuan Chi suggested that the lake became shallower, which was the result of the dry/cold conditions during the LIA (Cheng et al., 2020). Multiple proxies from Dajiuhu Lake consistently recorded a notable decreasing of rainfall between 500 and 150 yr BP (Ma et al., 2008). Therefore, the $\delta^{18}O$ and $\delta^{13}C$ records in BF4, together with other available climatic proxies, all suggest that dry/cold conditions prevailed at the cave site and surroundings during the LIA.

For mechanism, dry/cold conditions during the LIA are consistent with the Spörer and Maunder solar minima (Solanki et al., 2004; Fig. 6b), and warm phase of the ENSO/PDO (Shen et al., 2006; Donnelly and Woodruff, 2007; Fig. 6c). This correlation supports the idea that changes in solar activity played a key role in influencing monsoon climate changes, while the ENSO/PDO acted as a mediator to amplify and transmit the solar signal to the EASM domain (Emile-Geay et al., 2007). Furthermore, the climatic conditions during the LIA were timed with a negative phase of the Arctic Oscillation (AO; Chu et al., 2008; Fig. 6d), as well as cold phase of the Atlantic Multidecadal Oscillation (AMO; Mann et al., 2009; Fig. 6f). In the meantime, the SO_4 residuals recorded from Greenland ice cores show more active volcanic eruptions during the LIA (Mayewski et al., 1997; Fig. 6e). Therefore, the dry/cold conditions in central China during the LIA are likely to be attributed to a reduction in solar output and its associated impact on oceanic–atmospheric circulations. In addition, the volcanic eruptions, AMO, and AO may also have their own contributions (Cook et al., 2010; Wei et al., 2020). However, this dynamical interpretation is challenged by some facts. During the Maunder minima, reduced solar activity induced a positive shift of 1.8‰ in BF4 $\delta^{18}O$ value, whereas similar feedback was muted during the Spörer minima. This disharmony is partly attributed to the mediator's performance. The ENSO, AMO, and NAO (North Atlantic Oscillation) exhibited an anti-phase with the solar activity during the Maunder minima. The amplification effects are therefore eroded, resulting in a slight positive shift of the BF4 $\delta^{18}O$ value. Alternatively, the timing of the positive shifts of $\delta^{18}O$ and $\delta^{13}C$ values seems earlier than the onset of the Maunder minima. The plausible interpretation for this asynchrony is attributed to dating uncertainties in our record.

Previous studies have demonstrated that climatic changes may have important impacts on social evolution (Wu and Liu, 2004; Yancheva et al., 2007; Zhang et al., 2008; Tan et al., 2011; Xu et al., 2019). We counted the numbers of the military conflicts in China over the past 1000 years (Editorial Committee of Chinese Military History, 1985; Fig. 6i), and then compared them with the BF4 records. It is noted that the peak in military conflicts during dynastic transitions corresponds to abnormal shifts in the BF4 records. For example, the military conflicts in China were increased to approximately 80 between 400 and 200 yr BP, which were timed with the transition between the end of the Ming Dynasty and the initiation of the Qing Dynasty. At that time, a severe drought was recorded in the BF4 $\delta^{18}O$ record. The mentioned shift of 2‰ in the BF4 $\delta^{13}C$ record indicates that climatic conditions in central China were drier and colder. The close relationship in these records suggests that the serious social unrest at the end of the Ming Dynasty was probably related to climatic deterioration.

The collapse of the Ming Dynasty was mainly resulted from a combination of political, economic, and military factors. However, the non-social factors, such as the influence of climatic conditions cannot be neglected. In ancient times, the agricultural harvests relied heavily on

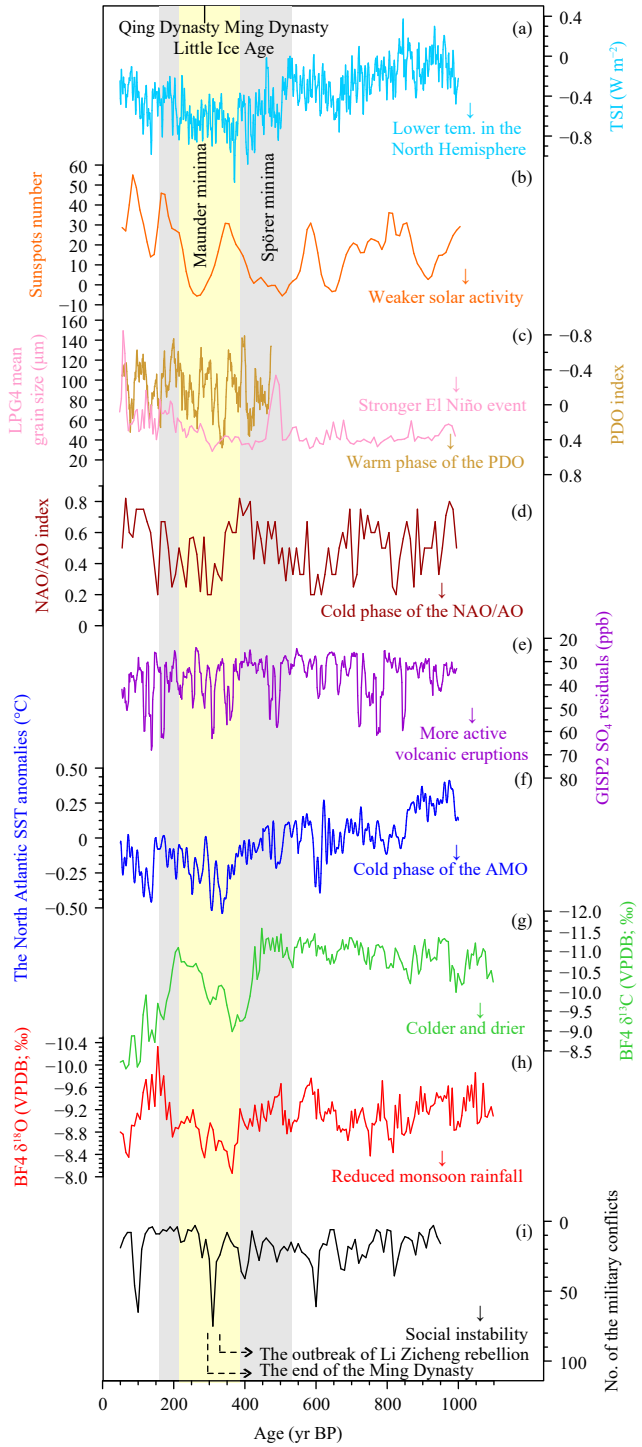

Fig. 6. The climatic deteriorations and social crisis during the LIA. (a) The reconstructed temperature in the NH (light blue curve; Mann and Jones, 2003), (b) sunspot number (SNN) record (orange curve; Solanki et al., 2004), (c) the reconstructed PDO index (gold curve; Shen et al., 2006) and ENSO activity (pink curve; Donnelly and Woodruff, 2007), (d) the reconstructed NAO index (ruby red curve; Chu et al., 2008), (e) the reconstructed AMO index as inferred from the North Atlantic STT variations (blue curve; Mann et al., 2009), (f) the volcanic actives as revealed by SO_4 residuals in Greenland ice cores (purple curve; Mayewski et al., 1997), (g) the local hydroclimate changes as revealed by the $\delta^{13}C$ record in BF4 (green curve; this study), (h) the enhanced monsoon rainfall in central China as revealed by the $\delta^{18}O$ record in BF4 (red curve; this study), and (i) the military conflicts in China as revealed by historical documents (black curve; Editorial Committee of Chinese Military History, 1985). The ancient dynasties that controlled China are indicated at the top of figure. The timing of the LIA is illustrated by a grey bar. The timing of the worst climatic event is illustrated by a yellow bar, which is coherent with a collapse of the Ming Dynasty and a victory of the Qing Dynasty.

climatic conditions due to their lower productivity. The severe droughts and temperature drops between 400 and 200 yr BP may have led to crop failures and then severe-famines, which may have fueled the great uprisings in central China. For example, the Li Zicheng rebellion started in the northwest of central China at approximately 320 yr BP. To maintain the dynastic rule, the military conflicts may have broken out between official-authorities and the general populations, resulting in massive deaths and the southward migration of the regional population. Consequently, the economy was destroyed, which may have seriously weakened the national power and accelerated the dynastic collapse at approximately 302 yr BP. Hence, our record suggests that climatic deterioration played an important role in causing the serious social unrest at the end of the Ming Dynasty, which ultimately contributed to China's social evolution.

5. Conclusions

The $\delta^{18}O$ and $\delta^{13}C$ records obtained from stalagmite BF4 from Xiniu Cave, central China, are used to reconstruct monsoon climate change for the past 4700 years. The long-term increasing trend of our $\delta^{18}O$ record since the late-Holocene is consistent with other hydroclimate records from monsoonal China and follows the gradually decreasing NHSI. This feature enables us to ascribe the $\delta^{18}O$ signal as a proxy of EASM rainfall. The $\delta^{13}C$ variation is locally dependent and is associated with regional rainfall and temperature change. Over the past 4700 years, a series of dry and wet periods, with cycles of ~470 and ~80 yr, were observed when the long-term trend of $\delta^{18}O$ record is removed. These centennial–decadal-scale climate changes are mainly caused by solar activity variation. The impact of solar activity is probably amplified by the ENSO/PDO. Other candidates in influencing the EASM changes, including the volcanic eruptions, AMO, and AO cannot be overlooked. By comparing our records with the historical records of military conflicts in China, the results provide an additional case that the peak climatic deterioration within the LIA may have a profound impact on China's social evolution.

Acknowledgments. We wish to thank the constructive suggestions from editors and three anonymous reviewers. In addition, Jingwei Zhang especially wish to thank Leina Wei, whose concerns have given his spiritual support over the past years.

REFERENCES

Asmerom, Y., V. Polyak, S. Burns, et al., 2007: Solar forcing of Holocene climate: New insights from a speleothem record, southwestern United States. *Geology*, **35**, 1–4, doi: 10.1130/G22865A.1.

Baker, A., E. Ito, P. L. Smart, et al., 1997: Elevated and variable values of ^{13}C in speleothems in a British cave system. *Chem. Geol.*, **136**, 263–270, doi: 10.1016/S0009-2541(96)00129-5.

Baldini, J. U. L., F. McDermott, A. Baker, et al., 2005: Biomass effects on stalagmite growth and isotope ratios: A 20th century analogue from Wiltshire, England. *Earth Planet. Sci. Lett.*, **240**, 486–494, doi: 10.1016/j.epsl.2005.09.022.

Berger, A., and M. F. Loutre, 1991: Insolation values for the climate of the last 10 million years. *Quat. Sci. Rev.*, **10**, 297–317, doi: 10.1016/0277-3791(91)90033-Q.

Breitenbach, S. F. M., K.Rehfeld, B. Goswami, et al., 2012: Constructing proxy records from age models (COPRA). *Climate Past*, **8**, 1765–1779, doi: 10.5194/cp-8-1765-2012.

Cai, Y. J., L. C. Tan, H. Cheng, et al., 2010: The variation of summer monsoon precipitation in central China since the last deglaciation. *Earth Planet. Sci. Lett.*, **291**, 21–31, doi: 10.1016/j.epsl.2009.12.039.

Chen, H., S. L. Guo, C. Y. Xu, et al., 2007: Historical temporal trends of hydro-climatic variables and runoff response to climate variability and their relevance in water resource management in the Hanjiang Basin. *J. Hydrol.*, **344**, 171–184, doi: 10.1016/j.jhydrol.2007.06.034.

Chen, W., 2002: Impacts of El Niño and La Niña on the cycle of the East Asian winter and summer monsoon. *Chinese J. Atmos. Sci.*, **26**, 595–610. (in Chinese)

Chen, W., J. Feng, and R. G. Wu, 2013: Roles of ENSO and PDO in the link of the East Asian winter monsoon to the following summer monsoon. *J. Climate*, **26**, 622–635, doi: 10.1175/JCLI-D-12-00021.1.

Cheng, B., J. Adams, J. H. Chen, et al., 2020: Neoglacial trends in diatom dynamics from a small alpine lake in the Qinling mountains of central China. *Climate Past*, **16**, 543–554, doi: 10.5194/cp-16-543-2020.

Cheng, H., R. L. Edwards, A. Sinha, et al., 2016: The Asian monsoon over the past 640,000 years and ice age terminations. *Nature*, **534**, 640–646, doi: 10.1038/nature18591.

Chu, G. Q., Q. Sun, X. H. Wang, et al., 2008: Snow anomaly events from historical documents in eastern China during the past two millennia and implication for low-frequency variability of AO/NAO and PDO. *Geophys. Res. Lett.*, **35**, L14806, doi: 10.1029/2008GL034475.

Cook, E. R., K. J. Anchukaitis, M. B. Buckley, et al., 2010: Asian monsoon failure and megadrought during the last millennium. *Science*, **328**, 486–489, doi: 10.1126/science.1185188.

Cosford, J., H. R. Qing, B. Eglington, et al., 2008: East Asian monsoon variability since the Mid-Holocene recorded in a high-resolution, absolute-dated aragonite speleothem from eastern China. *Earth Planet. Sci. Lett.*, **275**, 296–307, doi: 10.1016/j.epsl.2008.08.018.

Cosford, J., H. R. Qing, D. Mattey, et al., 2009: Climatic and local effects on stalagmite $\delta^{13}C$ values at Lianhua Cave, China. *Palaeogeogr. Palaeoclimatol. Palaeoecol.*, **280**, 235–244, doi: 10.1016/j.palaeo.2009.05.020.

Cui, Y. F., Y. J. Wang, H. Cheng, et al., 2012: Isotopic and lithologic variations of one precisely-dated stalagmite across the Medieval/LIA period from Heilong Cave, central China. *Cli-*

mate Past, **8**, 1541–1550, doi: 10.5194/cp-8-1541-2012.

Ding, Y. H., and J. C. L. Chan, 2005: The East Asian summer monsoon: An overview. *Meteor. Atmos. Phys.*, **89**, 117–142, doi: 10.1007/s00703-005-0125-z.

Ding, Y. H., D. Si, Y. J. Liu, et al., 2018: On the characteristics, driving forces and inter-decadal variability of the East Asian summer monsoon. *Chinese J. Atmos. Sci.*, **42**, 533–558, doi: 10.3878/j.issn.1006-9895.1712.17261. (in Chinese)

Dong, J. G., Y. J. Wang, H. Cheng, et al., 2010: A high-resolution stalagmite record of the Holocene East Asian monsoon from Mt Shennongjia, central China. *Holocene*, **20**, 257–264, doi: 10.1177/0959683609350393.

Donnelly, J. P., and J. D. Woodruff, 2007: Intense hurricane activity over the past 5,000 years controlled by El Niño and the West African monsoon. *Nature*, **447**, 465–468, doi: 10.1038/nature05834.

Dorale, J. A., and Z. H. Liu, 2009: Limitations of Hendy test criteria in judging the paleoclimatic suitability of speleothems and the need for replication. *J. Cave Karst Stud.*, **71**, 73–80.

Dorale, J. A., R. L. Edwards, E. Ito, et al., 1998: Climate and vegetation history of the midcontinent from 75 to 25 ka: A speleothem record from Crevice Cave, Missouri, USA. *Science*, **282**, 1871–1874, doi: 10.1126/science.282.5395.1871.

Editorial Committee of Chinese Military History, 1985: *Tabulation of Wars in Ancient China*. People's Liberation Army Press, Beijing, 150–151. (in Chinese)

Emile-Geay, J., M. Cane, R. Seager, et al., 2007: El Niño as a mediator of the solar influence on climate. *Paleoceanography*, **22**, PA3210, doi: 10.1029/2006PA001304.

Fairchild, I. J., C. L. Smith, A. Baker, et al., 2006: Modification and preservation of environmental signals in speleothems. *Earth Sci. Rev.*, **75**, 105–153, doi: 10.1016/j.earscirev.2005.08.003.

Foukal, P., C. Fröhlich, H. Spruit, et al., 2006: Variations in solar luminosity and their effect on the Earth's climate. *Nature*, **443**, 161–166, doi: 10.1038/nature05072.

Gray, L. J., J. Beer, M. Geller, et al., 2010: Solar influences on climate. *Rev. Geophys.*, **48**, RG4001, doi: 10.1029/2009RG000282.

Hendy, C. H., 1971: The isotopic geochemistry of speleothems-I. The calculation of the effects of different modes of formation on the isotopic composition of speleothems and their applicability as palaeoclimatic indicators. *Geochim. Cosmochim. Acta*, **35**, 801–824, doi: 10.1016/0016-7037(71)90127-X.

Hu, C. Y., G. M. Henderson, J. H. Huang, et al., 2008: Quantification of Holocene Asian monsoon rainfall from spatially separated cave records. *Earth Planet. Sci. Lett.*, **266**, 221–232, doi: 10.1016/j.epsl.2007.10.015.

IPCC, 2007: *Climate Change 2007: The Physical Science Basis. Contribution of Working Group I to the Fourth Assessment Reportof the Intergovernmental Panel on Climate Change*. Cambridge University Press, Cambridge.

Ishimura, T., U. Tsunogai, and F. Nakagawa, 2008: Grain-scale heterogeneities in the stable carbon and oxygen isotopic compositions of the international standard calcite materials (NBS 19, NBS 18, IAEA-CO-1, and IAEA-CO-8). *Rapid Commun. Mass Spectrom.*, **22**, 1925–1932, doi: 10.1002/rcm.3571.

Li, D. L., Z. N. Xiao, and L. Zhao, 2019: Preferred solar signal and its transfer in the Asian-Pacific subtropical jet region. *Climate Dyn.*, **52**, 5173–5187, doi: 10.1007/s00382-018-4443-5.

Li, P., M. H. Zhang, X. G. Kong, et al., 2010: A stalagmite-record of East Asian summer monsoon in the last 2000 years and its correlation with historical records. *Mar. Geol. Quat. Geol.*, **30**, 201–208, doi: 10.3724/SP.J.1140.2010.04201. (in Chinese)

Li, X. L., X. P. Cui, D. He, et al., 2018: Evaluation of the Heshang Cave stalagmite calcium isotope composition as a paleohydrologic proxy by comparison with the instrumental precipitation record. *Sci. Rep.*, **8**, 2615, doi: 10.1038/s41598-018-20776-5.

Li, Y. P., C. M. Ma, B. Zhou, et al., 2016: Environmental processes derived from peatland geochemistry since the last deglaciation in Dajiuhu, Shennongjia, central China. *Boreas*, **45**, 423–438, doi: 10.1111/bor.12168.

Ma, C. M., C. Zhu, C. G. Zheng, et al., 2008: High-resolution geochemistry records of climate changes since late-glacial from Dajiuhu peat in Shennongjia Mountains, Central China. *Chinese Sci. Bull.*, **53**, 28–41, doi: 10.1007/s11434-008-5007-6.

Maher, B. A., and R. Thompson, 2012: Oxygen isotopes from Chinese caves: Records not of monsoon rainfall but of circulation regime. *J. Quat. Sci.*, **27**, 615–624, doi: 10.1002/jqs.2553.

Mann, M. E., and P. D. Jones, 2003: Global surface temperatures over the past two millennia. *Geophys. Res. Lett.*, **30**, 1820, doi: 10.1029/2003GL017814.

Mann, M. E., Z. H. Zhang, S. Rutherford, et al., 2009: Global signatures and dynamical origins of the Little Ice Age and medieval climate anomaly. *Science*, **326**, 1256–1260, doi: 10.1126/science.1177303.

Mantua, N. J., S. R. Hare, Y. Zhang, et al., 1997: A Pacific interdecadal climate oscillation with impacts on salmon production. *Bull. Amer. Meteor. Soc.*, **78**, 1069–1080, doi: 10.1175/1520-0477(1997)078<1069:APICOW>2.0.CO;2.

Mattey, D., D. Lowry, J. Duffet, et al., 2008: A 53 year seasonally resolved oxygen and carbon isotope record from a modern Gibraltar speleothem: Reconstructed drip water and relationship to local precipitation. *Earth Planet. Sci. Lett.*, **269**, 80–95, doi: 10.1016/j.epsl.2008.01.051.

Mayewski, P. A., L. D. Meeker, M. S. Twickler, et al., 1997: Major features and forcing of high-latitude northern hemisphere atmospheric circulation using a 110,000-year-long glaciochemical series. *J. Geophys. Res. Oceans*, **102**, 26345–26366, doi: 10.1029/96JC03365.

McDermott, F., 2004: Palaeo-climate reconstruction from stable isotope variations in speleothems: A review. *Quat. Sci. Rev.*, **23**, 901–918, doi: 10.1016/j.quascirev.2003.06.021.

Meehl, G. A., P. R. Gent, J. M. Arblaster, et al., 2001: Factors that affect the amplitude of El Niño in global coupled climate models. *Climate Dyn.*, **17**, 515–526, doi: 10.1007/PL00007929.

Meehl, G. A., J. M. Arblaster, K. Matthes, et al., 2009: Amplifying the Pacific climate system response to a small 11-year solar cycle forcing. *Science*, **325**, 1114–1118, doi: 10.1126/science.1172872.

Moy, C. M., G. O. Seltzer, D. T. Rodbell, et al., 2002: Variability of El Niño/Southern Oscillation activity at millennial timescales during the Holocene epoch. *Nature*, **420**, 162–165, doi:

10.1038/nature01194.

Mudelsee, M., 2003: Estimating Pearson's correlation coefficient with bootstrap confidence interval from serially dependent time series. *Math. Geol.*, **35**, 651–665, doi: 10.1023/B:MATG.0000002982.52104.02.

Neff, U., S. J. Burns, A. Mangini, et al., 2001: Strong coherence between solar variability and the monsoon in Oman between 9 and 6 kyr ago. *Nature*, **411**, 290–293, doi: 10.1038/35077048.

Rasmusson, E. M., and T. H. Carpenter, 1983: The relationship between eastern equatorial Pacific sea surface temperatures and rainfall over India and Sri Lanka. *Mon. Wea. Rev.*, **111**, 517–528, doi: 10.1175/1520-0493(1983)111<0517:TRBEEP>2.0.CO;2.

Ropelewski, C. F., and M. S. Halpert, 1996: Quantifying Southern Oscillation–precipitation relationships. *J. Climate*, **9**, 1043–1059, doi: 10.1175/1520-0442(1996)009<1043:QSOPR>2.0.CO;2.

Shao, Q. F., C. H. Li, M. J. Huang, et al., 2019: Interactive programs of MC-ICPMS data processing for ^{230}Th/U geochronology. *Quat. Geochronol.*, **51**, 43–52, doi: 10.1016/j.quageo.2019.01.004.

Shen, C. M., W. C. Wang, W. Gong, et al., 2006: A Pacific decadal oscillation record since 1470 AD reconstructed from proxy data of summer rainfall over eastern China. *Geophys. Res. Lett.*, **33**, L03702, doi: 10.1029/2005GL024804.

Shi, H., and B. Wang, 2019: How does the Asian summer precipitation–ENSO relationship change over the past 544 years? *Climate Dyn.*, **52**, 4583–4598, doi: 10.1007/s00382-018-4392-z.

Solanki, S. K., I. G. Usoskin, B. Kromer, et al., 2004: Unusual activity of the Sun during recent decades compared to the previous 11,000 years. *Nature*, **431**, 1084–1087, doi: 10.1038/nature02995.

Spötl, C., I. J. Fairchild, and A. F. Tooth, 2005: Cave air control on dripwater geochemistry, Obir Caves (Austria): Implications for speleothem deposition in dynamically ventilated caves. *Geochim. Cosmochim. Acta*, **69**, 2451–2468, doi: 10.1016/j.gca.2004.12.009.

Steinhilber, F., J. Beer, and C. Fröhlich, 2009: Total solar irradiance during the Holocene. *Geophys. Res. Lett.*, **36**, L19704, doi: 10.1029/2009GL040142.

Stuiver, M., and B. Becker, 1993: High-precision decadal calibration of the radiocarbon time scale, AD 1950–6000 BC. *Radiocarbon*, **35**, 35–65, doi: 10.1017/S0033822200013801.

Tan, L. C., Y. J. Cai, Z. S. An, et al., 2011: Centennial-to decadal-scale monsoon precipitation variability in the semi-humid region, northern China during the last 1860 years: Records from stalagmites in Huangye Cave. *Holocene*, **21**, 287–296, doi: 10.1177/0959683610378880.

Tan, L. C., Y. J. Cai, H. Cheng, et al, 2018a: Centennial- to decadal-scale monsoon precipitation variations in the upper Hanjiang River region, China over the past 6650 years. *Earth Planet. Sci. Lett.*, **482**, 580–590, doi: 10.1016/j.epsl.2017.11.044.

Tan, L. C., Y. J. Cai, H. Cheng, et al, 2018b: High resolution monsoon precipitation changes on southeastern Tibetan Plateau over the past 2300 years. *Quat. Sci. Rev.*, **195**, 122–132, doi: 10.1016/j.quascirev.2018.07.021.

Tan, M., 2014: Circulation effect: Response of precipitation δ^{18}O to the ENSO cycle in monsoon regions of China. *Climate Dyn.*, **42**, 1067–1077, doi: 10.1007/s00382-013-1732-x.

Taylor, W. A., 2000: Change-Point Analysis: A Powerful New Tool for Detecting Changes. Available online at http://www.variation.com/cpa/tech/changepoint.html.

van Loon, H., and G. A. Meehl, 2012: The Indian summer monsoon during peaks in the 11 year sunspot cycle. *Geophys. Res. Lett.*, **39**, L13701, doi: 10.1029/2012GL051977.

Wang, B., and L. Ho, 2002: Rainy season of the Asian-Pacific summer monsoon. *J. Climate*, **15**, 386–396, doi: 10.1175/1520-0442(2002)015<0386:RSOTAP>2.0.CO;2.

Wang, J. S., and L. Zhao, 2012: Statistical tests for a correlation between decadal variation in June precipitation in China and sunspot number. *J. Geophys. Res.Atmos.*, **117**, D23117, doi: 10.1029/2012JD018074.

Wang, Y. J., H. Cheng, R. L. Edwards, et al., 2005: The Holocene Asian monsoon: Links to solar changes and North Atlantic climate. *Science*, **308**, 854–857, doi: 10.1126/science.1106296.

Wei, K., W. Chen, L. Y. Xu, et al., 2020: Stratosphere amplifies the global climate effect of wildfires. *Sci. China Earth Sci.*, **63**, 309–311, doi: 10.1007/s11430-019-9560-3.

Wu, W. X., and T. S. Liu, 2004: Possible role of the "Holocene Event 3" on the collapse of Neolithic cultures around the Central Plain of China. *Quat. Int.*, **117**, 153–166, doi: 10.1016/S1040-6182(03)00125-3.

Xiao, Z. N., and W. J. Huo, 2016: Influences of Solar Activity on Climate: The spatio-temporal selectivity of the amplification process. *Adv. Meteor. Sci. Technol.*, **6**, 141–147, doi: 10.3969/j.issn.2095-1973.2016.03.019. (in Chinese)

Xu, D. K., H. Y. Lu, G. Q. Chu, et al., 2019: Synchronous 500-year oscillations of monsoon climate and human activity in Northeast Asia. *Nat. Commun.*, **10**, 4105, doi: 10.1038/s41467-019-12138-0.

Yancheva, G., N. R. Nowaczyk, J. Mingram, et al., 2007: Influence of the intertropical convergence zone on the East Asian monsoon. *Nature*, **445**, 74–77, doi: 10.1038/nature05431.

Yu, L., 2013: Potential correlation between the decadal East Asian summer monsoon variability and the Pacific decadal oscillation. *Atmos. Ocean. Sci. Lett.*, **6**, 394–397, doi: 10.3878/j.issn.1674-2834.13.0040.

Yu, L., T. Furevik, O. H. Otterå, et al., 2015: Modulation of the Pacific Decadal Oscillation on the summer precipitation over East China: A comparison of observations to 600-years control run of Bergen Climate Model. *Climate Dyn.*, **44**, 475–494, doi: 10.1007/s00382-014-2141-5.

Zhang, H. L., K. F. Yu, J. X. Zhao, et al., 2013: East Asian Summer Monsoon variations in the past 12.5 ka: High-resolution δ^{18}O record from a precisely dated aragonite stalagmite in central China. *J. Asian Earth Sci.*, **73**, 162–175, doi: 10.1016/j.jseaes.2013.04.015.

Zhang, J. W., S. S. Liu, D. B. Liu, et al., 2019: Correlation between oxygen and carbon isotopes of speleothems from Tian'e Cave, central China: Insights into the phase relationship between Asian summer and winter monsoons. *J. Asian Earth Sci.*, **180**, 103884, doi: 10.1016/j.jseaes.2019.103884.

Zhang, J. W., X. G. Kong, K. Zhao, et al., 2020: Centennial-scale climatic changes in Central China during the Holocene climatic optimum. *Palaeogeogr. Palaeoclimatol. Palaeoecol.*, **558**, 109950, doi: 10.1016/j.palaeo.2020.109950.

Zhang, P. Z., H. Cheng, R. L. Edwards, et al., 2008: A test of climate, sun, and culture relationships from an 1810-year Chinese cave record. *Science*, **322**, 940–942, doi: 10.1126/science.1163965.

Zhang, W. C., H. Yan, J. Dodson, et al., 2018: The 9.2 ka event in Asian summer monsoon area: The strongest millennial scale collapse of the monsoon during the Holocene. *Climate Dyn.*, **50**, 2767–2782, doi: 10.1007/s00382-017-3770-2.

Zhang, W. H., S. T. Chen, Y. J. Wang, et al., 2019: Rapid change in the East Asian summer monsoon: Stalagmite records in Hubei, China. *Quat. Res.*, **39**, 765–774, doi: 10.11928/j.issn.1001-7410.2019.03.21. (in Chinese)

Zhao, K., Y. J. Wang, R. L. Edwards, et al., 2016: Contribution of ENSO variability to the East Asian summer monsoon in the late Holocene. *Palaeogeogr. Palaeoclimatol. Palaeoecol.*, **449**, 510–519, doi: 10.1016/j.palaeo.2016.02.044.

Zhao, L., Y. X. Zhu, H. W. Liu, et al., 2016: A stable snow–atmosphere coupled mode. *Climate Dyn.*, **47**, 2085–2104, doi: 10.1007/s00382-015-2952-z.

Zhao, L., J. S. Wang, H. W. Liu, et al., 2017: Amplification of the solar signal in the summer monsoon rainband in China by synergistic actions of different dynamical responses. *J. Meteor. Res.*, **31**, 61–72, doi: 10.1007/s13351-016-6046-6.

Zhou, Q., and W. Chen, 2012: Influence of the 11-year solar cycle on the evolution of ENSO-related SST anomalies and rainfall anomalies in East Asia. *Chinese J. Atmos. Sci.*, **36**, 851–862, doi: 10.3878/j.issn.1006-9895.2011.11162. (in Chinese)

Zhu, Z. M., J. M. Feinberg, S. C. Xie, et al., 2017: Holocene ENSO-related cyclic storms recorded by magnetic minerals in speleothems of central China. *Proc. Natl. Acad. Sci. USA*, **114**, 852–857, doi: 10.1073/pnas.1610930114.

Tech & Copy Editor: Zhirong CHEN